Incorporating Biomechanics into Architectural Tree Models

Julia Taylor-Hell
University of Calgary and Alias, Canada
jftaylor@alumni.uwaterloo.ca

Abstract

We present a method for creating tree models with realistically curved branches, useful in the portrayal of natural scenes. Instead of attempting to replicate a tree's final shape by observation, we obtain this shape as nature does – by considering the tree's development in the context of its environment. The final shape of the branches results from their growth in length, girth, weight and rigidity under the influence of gravity and tropisms. Using the framework of L-systems, we extend Jirasek's biomechanical simulation of a plant axis to correctly represent an entire tree. Our model also simulates the reaction wood which actively reorients a leaning branch by differentiating the wood production in angular portions of the branch cross-section. To obtain realistic and controllable tree architectures, we regulate growth elements in the model using functions based on botanical findings. We create a multi-year simulation of tree growth under environmental influences, obtaining a realistic tree shape at every stage of its development.

1. Introduction

Botanical trees are modelled extensively for the portrayal of natural scenes in the animation industry. Obtaining realistically shaped trees is a common goal in this field as well as in botanical research. An important shape characteristic of many trees seen in nature is the bending and curving of branches, as depicted in Figure 1. By simulating the botanical and biomechanical processes of the tree's development, we arrive at branch shapes similar to those seen in nature. In particular, the tree's response to gravity during its growth has a profound impact on the shape it develops.

Jirasek presented a biomechanical model of a growing plant axis which responds to gravity [10]. This paper extends her method to properly handle branching structures such as trees. Because complex and realistic models can be represented, these results are made more relevant to the Graphics community. Another important contribution of our model is in the simulation of reaction wood production to reorient a leaning branch.

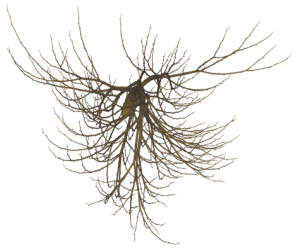

Figure 1. Biomechanical tree model

In order to properly visualize the influence of biomechanics on tree growth, we need to begin with a realistic tree architecture. In Section 3 we outline some botanical findings relevant to tree structure and describe our function-based approach for controlling tree architecture. In Section 4 we provide an in-depth description of the biomechanical simulation, reviewing Jirasek's method for single plant axes. Our extension of her model to branching structures and to trees in particular is presented in Section 5. The simulation of reaction wood is described in Section 6.

2 Previous work

General methods of modelling trees for computer graphics have been reviewed in the past [19]. Here we focus on the works related to biomechanics.

Several tree modeling systems in existence allow for simplified simulations of tropisms. These systems include Treemaker [2] and Xfrog [13], as well as L-studio's L-system modeling software [11]. However, none of these systems provide a rigorous physically accurate solution to the problem.

In [6], Fournier et al. present a biomechanical model using beams to simulate the bending of a plant stem due to loading and stresses. The authors describe the addition of radial layers, and the resulting stem is characterized by an "S" shape visible in many plant stems and depicted in Figure 5.

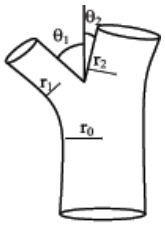

Figure 2. Cross-sectional radii and deviation angles of child branches

More recent advances make use of these results. Alméras et al. model a two-dimensional stem using bending beams [1]. Fourcaud et al. use the AMAP simulation software to create a finite element model composed of multi-layer deformable beams [4]. Radial layers are added to simulate thickening of the stem, and new beams are added to simulate stem lengthening.

Jirasek employs L-systems to create a biomechanical model of a growing plant stem that bends due to external forces [10]. Her model deals largely with single plant axes, with only a superficial extension to branching structures. This is because her approach relies on the assumption that all rotations occurring in the model are infinitesimal – as such the model cannot properly handle branching points. Her work was also limited by the complexity of the model's representation in CPFG, at that time the only available modelling framework for L-systems.

Recent progress in the realm of L-System languages has enabled further development of this approach. The L+C modelling language [12] makes two important improvements to the workings of L-systems which are relevant to modelling biomechanics. First, it allows user-defined structures to be passed as parameters to the L-system's modules. Also, L+C introduces *fast information transfer*, described in Section 6.4, by which a signal originating at one end of a structure can be propagated to the other end in a single rewriting step. This results in a significant speedup in our simulations, allowing for interactive frame rates and much more complex models.

3 Botanical findings and tree architecture

We first define some botanical terms. The *order* of a branch is the number of ancestors it has in the tree; a main trunk has order 0. We refer to a branch of order 1 as the daughter of the branch of order 0 from which it originated. In a growing tree, *primary growth* refers to the lengthening of branches as well as the production of buds, leaves and fruit. *Secondary growth* is the radial thickening that occurs so as to support the added load of new segments.

According to extensive measurements by Murray, the girth of a parent branch depends on the girths of its daughters according to the equation

$$r_0^P = r_1^P + r_2^P \quad (1)$$

where r is cross-sectional radius and P ranged between 2.49 for large trees and 3 for smaller trees [16]. Murray's findings were reinforced by theoretical reasoning with the *pipe model* of Shinozaki et al. [21]. This theory states that the number of leaves above any horizontal level on a tree is proportional to the cross-sectional area of all branches at that level.

Two angles are needed to describe lateral branching. The *deviation angle* is the angle θ made by a lateral branch relative to its parent's axis, as depicted in Figure 2. The *divergence angle*, ρ, specifies the position around the parent axis at which lateral growth occurs. In many trees, this angle ρ is the familiar 137.5° associated with *spiral phyllotaxis* [19]. Each new terminal bud formed along a branch is produced at a rotation of 137.5° beyond the previous bud.

Botanists refer to a section of branch grown in a single year as the *year growth increment*. Within this increment, many terminal buds are formed, some of which will become new shoots in the next year. Wilson notes that the probability of a bud becoming a shoot is higher for buds produced later in the year, so that the largest branches occur near the top of each growth increment [22]. He also notes that higher order branches elongate more slowly than those of lower order.

3.1 Functions specifying rules for architectural development

Our method allows botanical observations such as the above to be built into the model in the form of rules governing growth. We create a number of such rules using L-studio's graphically defined functions [12].

These functions can be called from within the model, using model parameters as input. The output of each function will be used to set the value of another architectural element. In this manner we can link two or more architectural traits which influence each other. For instance, Wilson's observation, above, links internode length to order of branching. Our model represents this rule as a function,

internode length = f(order)

which the user can manipulate graphically by moving control points on a curve. Often, more than one parameter controls the output – for instance, the *fate of a bud*, or its probability of becoming a shoot, depends on several factors.

bud shoots = ((f1(height in year)
** f2(order) * f3(parent length) * R) > 1)*

Figure 3. Two trees of different architectures, created by modifying graphical functions

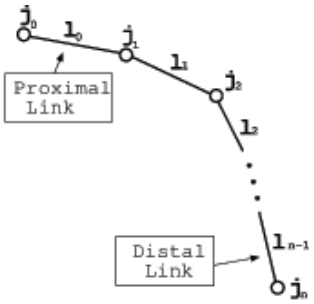

Figure 4. A mechanical manipulator with linked segments

Here, R is a random number incorporating randomness into the model, so that many different individuals can be created from the same tree species.

Functions such as these allow for user control over features of tree architecture. Manipulating the graphical functions allows users to represent many different tree architectures using the same model, as shown in Figure 3.

This framework for creating realistic tree architecture is used to describe the tree's genotype, while its phenotype is determined from the biomechanical simulation, as in [9].

4 Biomechanical model of a tree branch

First, we review the work of Jirasek on biomechanical modelling of unbranched plant axes or *stems*. We then present several extensions to her method.

Jirasek conceptualizes an individual plant axis as an elastic rod which may bend but not stretch. She models the bending of a stem by rotating a set of joints between small straight segments as in Figure 4. This representation is inspired by the concept of a *mechanical manipulator* robot described by Craig [3]. The model grows by appending new segments to its free end.

By convention, we call the links l_i, with i from 0 to n; l_0 is the root or *proximal* link, and l_n is the *distal* link, which is the tip of the stem. Link i is called the *parent* of link $i+1$. For simplicity, and because the segments are very small, we assume the mass m_i of each segment is located at its distal end. Between each pair of segments is a rotational joint with three degrees of freedom. In order to describe the relative properties of segments, we assign a three-dimensional orthogonal reference frame $\vec{H}\vec{L}\vec{U}$ to each segment as described in [20]. The long axis $\vec{l}$ of each segment always lies along its $\vec{H}$ vector. Thus, the $\vec{H}\vec{L}\vec{U}$ frame rotates along with the link.

Though the stem model is made up of discrete segments, these are small enough that we can conceptualize the stem as a continuously curved rod [18]. Thus, instead of defining angles of rotation between segments, the model uses a rate of rotation per unit length, $\vec{\Omega} = \frac{d\theta}{dl}$.

If the segment lengths are assumed to be very small, the joint rotations will therefore be infinitesimal. Infinitesimal rotations are known to commute, and as such can be expressed as vectors [14]. Consequently, the *rates* of these infinitesimal rotations can also be stored as vectors, as they will be used only in combination with small segment lengths. Thus $\vec{\Omega}$ may be expressed as a vector, whose direction gives the axis of rotation for a joint, and whose magnitude gives the angle of rotation, in radians per unit length of the segment.

Along a single axis, the child segment's orientation $\vec{H}_i$ is determined from the parent's orientation $\vec{H}_{i-1}$ using the rotational velocity vector $\vec{\Omega}_{i-1}$ of the parent link. Jirasek et al. perform this rotation using the vector cross-product [18],

$$\vec{H}_i' = \vec{H}_{i-1} + (\vec{\Omega}_{i-1} \times \vec{l}_{i-1}) \qquad (2)$$

which is acceptable since her model assumes infinitesimal rotations. Our model will perform all rotations using quaternions, so as to properly handle the non-infinitesimal rotations at branching points. The details of our approach are described in Section 5.

The approach of Jirasek et al. also defines a rest, or preferred, rotational velocity $\underline{\vec{\Omega}}$ [18]. This is the stem's rate of rotation in the *unloaded state*, when it is not experiencing any torque due to gravity. It will be responsible for taking into account the effects of *negative geotropism*, defined below.

A *tropism* is a preferred direction of growth in a plant in response to environmental stimuli [22]. *Geotropism* refers to directed growth in reaction to gravity. In particular, *negative geotropism* accounts for the tendency of a new shoot to orient itself in an erect position, against the pull of gravity.

Clearly, the effects of self-weight and negative geotropism oppose each other: negative geotropism causes new growth to curve upward, while gravity pulls the existing stem downward. The result of these competing influ-

Figure 5. "S" shape of a stem due to self-weight and negative geotropism

ences is the sigmoidal shape predicted in [6]. A stem under such conditions, produced by our model, is shown in Figure 5.

These two effects of self-weight and negative geotropism are simulated by calculating the torques they exert on each segment. The gravitational torque $\vec{\tau}_i$ acting on each segment i is due to the total overhanging mass M_i it supports [10]:

$$\vec{\tau}_i = \vec{l}_{i+1} \times (\vec{g} * M_{i+1}) \; + \; \vec{\tau}_{i+1} \tag{3}$$

The second torque acting on segment i as a result of negative geotropism is determined using a force vector, $\vec{F}^{tropic}$ which indicates the direction (up) and the intensity of this tropism:

$$\vec{\tau}_i^{tropic} = \vec{l}_{i-1} \times \vec{F}^{tropic} \tag{4}$$

These two torques $\vec{\tau}_i$ and $\vec{\tau}_i^{tropic}$ influence the rotational velocity of each segment. $\vec{\tau}_i$ is used in computing an update value for $\vec{\Omega}$.

$$\vec{\Omega}' = \frac{\vec{\tau}}{\Re} \tag{5}$$

and $\vec{\tau}_i^{tropic}$ is used to initialize the preferred rotational velocity $\underline{\vec{\Omega}}$ of a new segment:

$$\underline{\vec{\Omega}} = \frac{\vec{\tau}_i^{tropic}}{\Re} \tag{6}$$

Both of these equations depend on the *rigidity* $\Re$ of a rod, or its resistance to deformation. *Flexural rigidity* $\Re_f$ is resistance to bending, and depends on the strength of the material as specified by its Young's modulus E and the shape of the cross-section as determined by its moment of area I. In general, flexural rigidity is dependent upon the direction in which torque is applied, and as such it is a tensor quantity. However, if we assume that the rod's cross-section is circular (so that I is constant along any direction of bending in the plane of the cross-section) and that its material is isotropic and homogeneous (so that E is constant), flexural rigidity may be represented as a scalar. These assumptions simplify many calculations.

Therefore, the flexural rigidity of a segment is $\Re_f = E\,I$. To represent a tree stem, we use the values $E_{wood} = 10\,GPa$ for green wood [17], and $I_{circle} = \frac{\pi r^4}{4}$ for a circular cross-section of radius r.

Torsional rigidity is an object's resistance to twist. It is calculated similarly, using the equivalent constants for the case of torsion: $\Re_t = G\,J$, where G is the shear modulus and J is the polar moment of area, $J_{circle} = \frac{\pi}{2} r^4$ for a circular cross-section.

When dividing by rigidity $\Re$ as in Equations 6 and 5, the $\vec{H}$ component is divided by the torsional rigidity $\Re_t$ and the $\vec{L}$ and $\vec{U}$ components are divided by the flexural rigidity $\Re_f$.

4.1 Bidirectional propagation of information

Some of the model's biomechanical properties are dependent on values from neighbouring distal segments, and some on values from proximal segments. For this reason, the model requires both *forward propagation* (accumulating information toward the distal end of the stem) and *backward propagation* (toward the proximal end), to obtain information from both directions. The model performs forward and backward passes in alternation, so that values calculated in one direction can immediately influence those in the other direction. This *relaxation cycle* of forward and backward passes continues until the state values converge to equilibrium.

Because the model uses a relaxation method, it does not replace the value of $\vec{\Omega}$ at each step. Rather, it uses $\vec{\Omega}'$ along with the rest rotation rate $\underline{\vec{\Omega}}$ to update the existing value, using the following update formula:

$$\vec{\Omega} = (1-\alpha)\vec{\Omega} + \alpha(\underline{\vec{\Omega}} + \vec{\Omega}'). \tag{7}$$

Here, $\vec{\Omega}$ is updated to include a linear combination of the old $\vec{\Omega}$ value and a new value, which is the rest rotational velocity plus displacement caused by torque. The parameter α controls the speed of convergence to the new solution and may be reduced to prevent numerical instability.

4.2 Adding a segment

Adding a new distal segment affects previous segments in several ways. First, the weight of the new segment increases the torque acting on all previous segments as in Equation 3 . Secondly, all previous segments must grow *radially*, or in girth, according to the pipe model. Radial growth of a stem occurs by adding rings, or layers of wood, around the existing rod [6]. These layers increase rigidity and also reinforce the current shape of the stem. An older, bulkier stem is therefore less likely to change its curvature

even if there were a sudden change in the external forces in the system. This phenomenon is called *branch shape memory* [5].

Jirasek et al. calculate the new rest rotational velocity $\underline{\vec{\Omega}}'$ for the thickened stem by considering both the $\underline{\vec{\Omega}}$ value of the current stem and that of the new outer ring being added [18]:

$$\underline{\vec{\Omega}}' = \frac{\Re\, \underline{\vec{\Omega}} \;+\; \Re_{ring}\, \underline{\vec{\Omega}}_{ring}}{\Re + \Re_{ring}} \tag{8}$$

Because new radial growth reinforces the current shape of the stem, the rest curvature of the outer ring $\underline{\vec{\Omega}}_{ring}$ reflects the existing curvature of the stem:

$$\underline{\vec{\Omega}}_{ring} = \vec{\Omega} \tag{9}$$

The ring's rigidity is calculated as $\Re_{ring} = E_{juv} + I_{ring}$, where $I_{ring} = \frac{\pi}{4}(r_{out}^4 - r_{in}^4)$. The values r_{out} and r_{in} measure the distance from the center of the circle to the inner and outer edges of the ring, respectively. The stem's new total rigidity becomes the combined rigidity of the inner core and outer layer, $\Re + \Re_{ring}$.

5 Lateral branching

The problem of representing a curved plant stem becomes even more interesting when we allow for lateral branching. In this section we describe the extension to Jirasek's model which correctly represents branching structures instead of only single stems. To correctly compound these non-infinitesimal branching rotations with the rotations due to biomechanics, we perform all rotations using quaternions.

5.1 Branching points

Modifying a child segment's orientation to account for branching angles involves simulating phyllotaxis by spiralling around the $\vec{H}$ axis by the divergence angle ρ and then rotating by the deviation angle θ. Because these are non-infinitesimal rotations, we perform them using quaternions.

$$\begin{aligned}
\text{qDivergence} &= \text{new Quaternion}(\vec{H}_{i-1}, \rho) \\
\vec{N} &= \text{qDivergence}^{-1} * \vec{U}_{i-1} * \text{qDivergence} \\
\text{qDeviation} &= \text{new Quaternion}(\vec{N}, \theta) \\
\text{qBranching} &= (\text{qDivergence} * \text{qDeviation}) \\
\vec{H}_i &= \text{qBranching}^{-1} * \vec{H}_{i-1} * \text{qBending}
\end{aligned}$$

Equation 2 assumed a continuously curved rod with infinitesimal rotations, and therefore used the vector cross-product [18]. At branching points, however, our simulation needs to compose these biomechanical rotations with the above branching rotations, we must rephrase equation 2 in terms of quaternions.

Recall from Section 4 that the rotational velocity $\vec{\Omega}$ specifies a rotation per unit *length*. For each unit length of the parent segment, we rotate around axis $\frac{\vec{\Omega}}{\|\vec{\Omega}\|}$ by angle $\|\vec{\Omega}\|$. Thus the total rotation due to a parent segment of length $|\vec{l}_{i-1}|$ is by angle $\|\vec{\Omega}\| * |\vec{l}_{i-1}|$ around the same axis. We use this axis and angle to define a quaternion *qBending*.

$$\text{Quaternion qBending}(\frac{\vec{\Omega}_{i-1}}{\|\vec{\Omega}_{i-1}\|},\ \|\vec{\Omega}_{i-1}\| * |\vec{l}_{i-1}|) \tag{10}$$

Then, the reorientation due to the combined effects of branching and biomechanics becomes

$$\text{Quaternion qComplete} = (\text{qBranching} * \text{qBending}) \tag{11}$$

$$\vec{H}_i = \text{qComplete}^{-1} * \vec{H}_{i-1} * \text{qComplete} \tag{12}$$

A parent branch just before a bifurcation must accumulate the mass, girth, and torque information from both child branches. This is accomplished using the following formulae:

$$r_{i-1} = \sqrt[P]{r_i^{L^P} + r_i^{R^P}} \tag{13}$$

$$M_{i-1} = m_{i-1} + \sqrt[P]{M_i^{L^P} + M_i^{R^P}} \tag{14}$$

$$\vec{\tau}_{i-1} = (\vec{\tau}_i^L + \vec{\tau}_i^R) \tag{15}$$

where P is the pipe model constant, usually ranging between 2.49 for large trees to 3.0 for smaller trees [16]. Superscripts L and R represent left and right children.

6 Accurate simulation of wood behaviour

In this section we discuss our model's simulation of wood's behaviour. We improve our model's biological realism by simulating the evolution of wood's mechanical properties as it ages, as well as its active reorientation due to the formation of reaction wood.

6.1 Wood aging

Instead of using one value of Young's modulus E uniformly in the model, a more realistic simulation accounts for the stiffening of wood as it matures. Fournier describes the younger *sapwood*, which forms new rings under the bark, as being more supple than the *heartwood* at the centre of an older branch [5]. We therefore use a lower value of Young's modulus for *juvenile* wood as compared to *mature* wood. When a new shoot is formed, we use the lower juvenile wood stiffness E_{juv} to describe the suppleness of new sapwood. As the internal heartwood ages, it undergoes a gradual stiffening as Young's modulus approaches E_{mature}. The heartwood's E value is computed using the appropriate linear combination of E_{juv} and E_{mature}. The newly added sapwood in the radial layer has a Young's modulus of E_{juv} .

Figure 6. Photograph of trunk straightening due to reaction wood

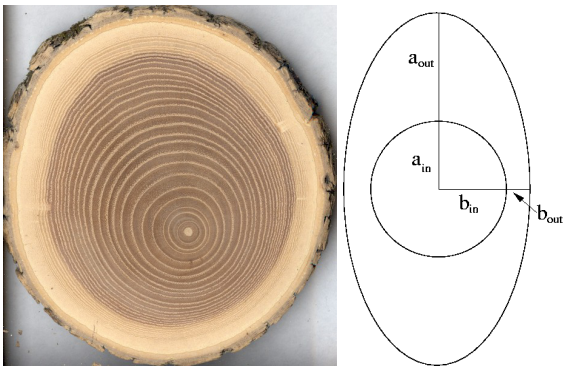

Figure 7. (a) Asymmetrical thickening of rings due to reaction wood, with permission from [7] (b) Circular inner core with new elliptical reaction wood ring

6.2 Reaction wood

In the model described so far, a trunk which begins to lean due to self-weight has no way to correct the imbalance and return to an upright orientation. Yet, straightenings of leaning trunks are indeed observed in nature, as shown in Figure 6. This is due to active reorientation via secondary growth in the form of *reaction wood*.

Botanical studies have shown that reaction wood forms when a growing shoot deviates too far from an *equilibrium position* EP [17, 6]. To create reaction wood, leaning branches differentiate their wood production to create *angular dissymmetry* in the cross-section, both in the new wood's growth speed and in its material properties. Reaction wood also introduces growth strains which work to reorient an inclined branch.

Reaction wood grows faster than regular wood, forming thicker portions of new rings on the upper side of a branch in broad-leafed trees and on the lower side in conifers [15]. By thickening the appropriate angular section of the branch's new rings, reaction wood ovalizes the branch cross-section, as seen in Figure 7(a). This dissymmetry shifts the geometric center of the branch, and reduces the stress felt in the reaction wood zone by spreading the stress over a larger area.

Reaction wood also exhibits different mechanical properties than regular wood: it is optimized to resist compression in conifers, and to resist tension in broad-leafed trees [15]. In both cases, the result is that reaction wood is better able to resist further bending in the branch.

This differentiated growth produces growth stresses in the branch. These lead to growth strains which supply the moment needed to correct a lean by counteracting existing strains due to loading [17].

Hart et al. have simulated reaction wood by uniformly increasing girth at branching points, to resist a rotational force [9]. The authors have also modelled the effect of reaction wood on tree shape at branching points, using implicit surfaces [8]. The dissymmetry of material properties is not simulated in their biomechanical model, however, nor are the growth strains which cause righting of the branch.

Our model simulates each of the above-described properties of reaction wood. First, we detect a lean by recognizing a large deviation from EP. We consider a segment's EP to be its $\vec{\underline{\Omega}}$ value, and compare this with its current $\vec{\Omega}$ value to determine the magnitude of the deviation from EP. If the deviation exceeds a user-controllable threshold ξ, the production of reaction wood is triggered. All changes to the wood production intended to correct a lean must occur only in the new layers formed after the detection of the lean. The cross-section of the radial ring produced by reaction wood is thickened along the direction of bending. Since the ring, and consequently the entire branch, is no longer circular in cross-section, we replace the moments of area I_{circle} and I_{ring} with their counterparts for elliptical shapes:

$$I_{ellipse_a} = \frac{\pi}{4} a^3 b \quad (16)$$

$$I_{ellipticalRing_a} = \frac{\pi}{4}(a_{out}^3 b_{out} - a_{in}^3 b_{in}) \quad (17)$$

In these equations, a is the longer semi-axis of the ellipse, which lies in the direction of bending, and b is the shorter semi-axis. For simplicity, we assume that the longer semi-axis of the inner core a_{in} lies in the same direction as a_{out}, as in Figure 7(b). In other words, we assume that the axis of bending in the branch has not changed while reaction wood was being produced.

Note that, since the cross-section is no longer circular, flexural rigidity now differs along directions a and b. Equations 16 and 17 are used to calculate rigidity in the direction of bending, along a. The moment of area values used to calculate rigidity in the direction perpendicular to bending,

along b, are obtained by cubing the b term instead of the a term in these equations. The torsional rigidity also changes to use the J value for an elliptical cross-section, $J = \frac{\pi\, a^3\, b^3}{a^2+b^2}$.

To simulate the different mechanical properties of reaction wood, we use a larger Young's modulus E_{rw} in reaction wood than that which is used for regular secondary growth. To set the E value for the new ring, we estimate from Figure 7 that half of the new ring's wood is reaction wood:

$$E_{ring} = \frac{1}{2}E_{rw} + \frac{1}{2}E_{juv} \tag{18}$$

These alterations to the shape and stiffness of reaction wood serve to slow or even stop bending. Yet they cannot actually reverse the direction of bending to correct a lean. The third aspect of the reaction wood model simulates the growth strains which, in nature, provide rotational moment for the righting of a branch. We accomplish this by adjusting the rest curvature $\underline{\vec{\Omega}}_{ring}$ of the new ring in the direction opposite to the lean. The $\underline{\vec{\Omega}}$ value of the inner core of the branch tells us its desired curvature in the absence of load, so an adjustment toward $\underline{\vec{\Omega}}$ will act counter to the lean. The higher the proportion of reaction wood, $\beta \in [0,1]$, the more heavily we use $\underline{\vec{\Omega}}$ in setting the rest curvature of the ring:

$$\underline{\vec{\Omega}}_{ring} = (1-\beta)\,\vec{\Omega} + \beta\,\underline{\vec{\Omega}}. \tag{19}$$

This method captures reaction wood's tendency to reorient a leaning branch. The value of $\underline{\vec{\Omega}}_{ring}$ will influence the rest curvature of the entire segment, as expressed in Equation 8.

6.3 Seasons, leaves and fruit

To better replicate a tree's real environment, our simulation undergoes seasonal changes. Each year contains a summer, a winter and a spring. In summer, both primary and secondary growth occur. Newly created buds may host leaves and fruit, whose masses add to the supported weight of the parent internode. In winter, leaves and fruit are shed, and the tree branches are observed to spring back up slightly because of the reduced load, as seen in Figure 8. In the spring, the fate of the previous year's buds is determined; they will either abort or become new shoots according to architectural rules such as those described in Section 3.1.

6.4 L-System expression

L-systems are well-suited to express the problem of biomechanical plant growth. An in-depth description of L-systems can be found in [19]. An L-system represents a growing structure as a string of modules. Each module contains parameters which store information and allow for its communication to neighbor modules as *context*. At every *rewriting step*, each module is transformed according to a matching *production rule*. This process serves to expand the string of modules, resulting in the growth of the model when the modules are interpreted visually.

Figure 8. (a) A fruit tree in summer, bearing the load of fruit and leaves (b) In winter, under reduced load

In our simulation, we use a module's parameters to store the list of physical properties described above. These will be available to the proximal or distal neighbors through left or right context. This allows us to propagate information forward or backward across the branch.

Normally, the context in a production comes from the state of the module at the *previous* step. This information is, by nature, one step out of date. Thus, to propagate a signal across a branch of length n would require n rewriting steps. This results in very slow signal propagation, and slow convergence to the static equilibrium state.

However, the new L-system framework *LPFG* now allows for *fast information transfer* [12], which can propagate this same signal in a single rewriting step. Instead of using context from the previous rewriting step, we can access already-interpreted modules for the current step to obtain up-to-date information. Using this *new context* allows us to propagate a signal across the entire branch, regardless of its length, in a single rewriting step. This makes for a very efficient simulation; in fact, we obtain interactive rates for this simulation until the tree structure reaches a certain complexity.

7 Results and conclusions

The importance of biomechanics in determining tree shape is made evident in Figure 9. Image (a) provides the inspiration for the model. The effect of the biomechanics simulation is seen by comparing image (c) with image (b), which is the same architectural model without the biomechanics.

In this paper, we have extended Jirasek's biomechanical model of plant axes to branching structures so that we may accurately model growing trees. We have presented a botanically-based simulation of reaction wood and wood aging, as well as a mechanism to control tree architecture

(a) (b) (c)

Figure 9. (a) Inspiration from nature (b) Model without biomechanics (c) Model with biomechanics

with user-definable functions. The result is a sophisticated and controllable tree model which behaves realistically on both a physical and a botanical level.

The author thanks Dr. Przemyslaw Prusinkiewicz for his guidance with this project, as well as the National Sciences and Engineering Research Council of Canada.

References

[1] T. Alméras, J. Gril, and E. Costes. Bending of apricot tree branches under the weight of axillary growth. *Trees: Structure and Function*, 16(3):5–15, 2002.

[2] B. Bosanac and P. Zanchi, 2005. http://www.onyxtree.com.

[3] J. Craig. *Introduction to Robotics, Mechanics and Control*. Addison-Wesley, 1989.

[4] T. Fourcaud and P. Lac. Numerical modelling of shape regulation and growth stresses in trees. *Trees-Structure and Function*, 17:23–30, 2002.

[5] M. Fournier. Mécanique de l'arbre. maturation, poids propre, contraintes climatiques. *Thèse de Doctorat, Institut National Polytechnique de Lorraine*, 1989.

[6] M. Fournier, H. Bailleres, and B. Chanson. Tree biomechanics: Growth, cumulative prestresses, and reorientations. *Biomimetics*, 2(3):229–251, 1994.

[7] H. Grissino-Mayer, 2004. http://web.utk.edu/∼grissino/gallery.htm.

[8] J. Hart and B. Baker. Implicit modeling of tree surfaces. *Proceedings of the 1996 workshop on implicit surfaces*, 1996.

[9] J. Hart, B. Baker, and J. Michaelraj. Structural simulation of tree growth and response. *The Visual Computer*, 19:151–163, 2003.

[10] C. A. Jirasek. A biomechanical model of branch shape in plants expressed using L-systems. *Master's Thesis, University of Calgary*, 2000.

[11] R. Karwowski and P. Prusinkiewicz. The L-system-based plant-modeling environment L-studio 4.0. *Proceedings of the 4th International Workshop on Functional-Structural Plant Models*, pages 403–405.

[12] R. Karwowski and P. Prusinkiewicz. Design and implementation of the L+C modeling language. *Electronic Notes in Theoretical Computer Science*, 86(2), 2003.

[13] B. Lintermann and O. Deussen. Interactive modeling of plants. *IEEE Computer Graphics and Applications*, 19(1), 1999.

[14] J. Marion and S. Thornton. *Classical Dynamics of Particles and Systems*. Harcourt Brace Jovanovich, 3 edition, 1988.

[15] C. Mattheck. *Design in Nature: Learning from Trees*. Springer-Verlag, 1998.

[16] C. Murray. A relationship between circumference and weight in trees and its bearing on branching angles. *Journal of General Physiology*, 10:725–729, 1927.

[17] K. J. Niklas. *Plant Biomechanics: An Engineering Approach to Plant Form and Function*. University of Chicago Press, 1992.

[18] P. Prusinkiewicz, C. A. Jirasek, and B.Moulia. Integrating biomechanics into developmental plant models expressed using L-systems. *Plant biomechanics*, 191:615–624, 1998.

[19] P. Prusinkiewicz and A. Lindenmayer. *The Algorithmic Beauty of Plants*. Springer, 1996.

[20] P. Prusinkiewicz, L. Mündermann, R. Karwowski, and B. Lane. The use of positional information in the modelling of plants. In *Proceedings of SIGGRAPH*, pages 289–300, 2001.

[21] K. Shinozaki, K. Yoda, K. Hozumi, and T. Kira. A quantitative analysis of plant form - the pipe theory model. *Japanese Journal of Ecology*, 14(3):97–105, 1964.

[22] B. F. Wilson. *The Growing Tree*. University of Massachusetts Press, 1984.